Evaluation of the use of second generation wavelets in the Coherent Vortex Simulation approach

By D. E. Goldstein†, O. V. Vasilyev†, A. A. Wray‡ AND R. S. Rogallo‡

The objective of this study is to investigate the use of the second generation bi-orthogonal wavelet transform for the field decomposition in the Coherent Vortex Simulation of turbulent flows. The performances of the bi-orthogonal second generation wavelet transform and the orthogonal wavelet transform using Daubechies wavelets with the same number of vanishing moments are compared in *a priori* tests using a spectral direct numerical simulation (DNS) database of isotropic turbulence fields: 256^3 and 512^3 DNS of forced homogeneous turbulence ($Re_\lambda = 168$) and 256^3 and 512^3 DNS of decaying homogeneous turbulence ($Re_\lambda = 55$). It is found that bi-orthogonal second generation wavelets can be used for coherent vortex extraction. The results of *a priori* tests indicate that second generation wavelets have better compression and the residual field is closer to Gaussian. However, it was found that the use of second generation wavelets results in an integral length scale for the incoherent part that is larger than that derived from orthogonal wavelets. A way of dealing with this difficulty is suggested.

1. Introduction

A new adaptive second generation wavelet collocation method for DNS of turbulent flows has recently been developed (Vasilyev & Bowman (2000), Kevlahan *et al.* (2000)). The adaptive wavelet collocation method is appropriate for high Reynolds number turbulence since wavelets (which are localized in both space and scale) adapt the numerical resolution naturally to the intermittent structure of turbulence at small scales. The wavelet method thus allows turbulent flows to be calculated with a greatly reduced number of modes with little loss in accuracy. Furthermore, the computational cost of the algorithm is independent of the dimensionality of the problem and is $O(\mathcal{N})$, where $\mathcal{N}$ is the total number of collocation points actually used in the simulation.

The efficiency of the adaptive wavelet collocation method can be greatly enhanced by combining it with the recently developed Coherent Vortex Simulation (CVS) approach (Farge *et al.* (1999)), which is closely related to the standard large eddy simulation (LES) method. In contrast to LES, in which the velocity field is decomposed into large- and small-scale fields, in CVS the velocity field is decomposed into coherent (filtered) and incoherent (residual) fields. The filtered scales, which represent the coherent non-Gaussian part of the flow, are obtained numerically from the filtered vorticity-transport equation, while the effect of the residual scales, which represent the incoherent Gaussian part of the flow, needs to be modeled. The success of the CVS approach depends on how close the residual field is to Gaussian white noise and how few modes are required for

† University of Missouri-Columbia
‡ NASA Ames Reserach Center, Moffett Field, CA

the filtered field representation. It was shown by Donoho (1993) that wavelet coefficient thresholding is an optimal method for separating Gaussian white noise from a signal. Thus the filtering can be performed in wavelet space using wavelet coefficient thresholding, which can be considered as a non-linear filter that depends on each flow realization. This wavelet filtering is achieved by performing the following three steps:

1. Perform the forward wavelet transform of $\vec{\omega}$.
2. Set to zero those wavelet coefficients, whose magnitude is below the given *a priori* prescribed threshold ϵ, *i.e.* $||\vec{\tilde{\omega}}||_2 \leq \epsilon$, where $\vec{\tilde{\omega}}$ is the wavelet transform of $\vec{\omega}$.
3. Apply the inverse wavelet transform.

As a result of this operation, the filtered vorticity field can be captured by a small fraction of the wavelet coefficients. The anticipated advantages of CVS over current methods are, first, the use of wavelet bases to significantly compress the vorticity field and so require simulation of only a small fraction of the degrees of freedom (those that contain a significant amount of energy and enstrophy), and second, one can presumably model the discarded modes more accurately than in LES since they are closer to Gaussian white noise than those resulting from the linear low pass filters used in LES. Initial work done by Farge *et al.* (1999) on a two-dimensional CVS method shows significant potential. It is anticipated that CVS applied to three-dimensional turbulent flows will provide substantial improvements in computational speed and accuracy over existing methods.

The final goal of our work is to develop a 3D CVS code that is able to simulate realistic scientific and engineering problems in complex domains. An adaptive wavelet collocation solver (Vasilyev & Bowman (2000), Kevlahan *et al.* (2000)) will be used to numerically solve the CVS equations on the adaptive grid. This adaptive wavelet collocation solver uses second generation bi-orthogonal wavelets, enabling it to solve problems in complex domains. It would be logical to use the same second generation wavelets for both the vorticity field filtering and the wavelet collocation solver. However, the use of second generation bi-orthogonal wavelets for coherent field extraction has not been explored up to now. Therefore, the objective of this study is to investigate in *a priori* tests the use of these wavelets only for the filtering of the vorticity field for coherent vortex extraction.

The rest of this paper is organized as follows. Section 2 gives a brief introduction to second generation wavelets. The CVS approach is then introduced in Section 3. Finally, in Section 4 results are presented of a parametric study of two different wavelet transforms applied to both forced and decaying homogeneous turbulence fields.

2. Second generation wavelets

Wavelets are basis functions which are localized in both physical space (due to their finite support) and wavenumber space (*e.g.* Fig. 1). In contrast, the Fourier transform is based on functions (sines and cosines) that are well localized in frequency but do not provide localization in physical space due to their global support. Because of this space/scale localization, the wavelet transform provides both spatial and scale (frequency) information while the Fourier transform only provides frequency information.

Although the wavelet transform with its space/scale localization is an attractive technique to apply to the solution of problems with localized structures such as the simulation of turbulent flows, traditional wavelet transforms have difficulties dealing with boundaries. Traditionally, wavelets ψ_k^j are defined as translates and dilates of one basic wavelet ψ, *i.e.* $\psi_k^j(x) = \psi(2^j x - k)$. These first generation wavelets are defined either in infinite or periodic domains.

Second generation wavelets (Sweldens (1996), Sweldens (1998)) are a generalization of first generation wavelets (Daubechies (1988), Cohen *et al.* (1992)) that supplies the necessary freedom to deal with complex geometries, arbitrary boundary conditions, and irregular sampling intervals. Second generation wavelets form a Reisz basis for some function space, with the wavelets being local in both space and frequency and often having many vanishing polynomial moments, but without the translation and dilation invariance of their first generation cousins. Despite the loss of these two fundamental properties of wavelet bases, second generation wavelets retain many of the useful features of first generation wavelets, including a fast $O(N)$ transform.

The construction of second generation wavelets is based on the lifting scheme that is discussed in detail in Sweldens (1996), Sweldens (1998). Here we just summarize the main advantages of second generation wavelets:

1. Wavelets are constructed in the spatial domain and can be custom designed for complex multi-dimensional domains and irregular sampling intervals.
2. No auxiliary memory is required and the original signal can be replaced with its wavelet transform.
3. The second generation wavelet transform is a factor of two faster than the first.
4. With lifting, the inverse wavelet transform is constructed by simply reversing the order of operations and interchanging addition and subtraction operations.
5. The programming of the second generation wavelet transform is considerably simpler.
6. Second generation wavelets are naturally suitable for wavelet collocation methods, which have been shown to be superior to the wavelet Galerkin approach in handling general boundary conditions and nonlinearities in the equations.

For this study we use a set of second generation wavelets known in the literature as lifted interpolating (LI), or Donoho, wavelets (Sweldens (1996), Vasilyev & Bowman (2000)). In particular, *a priori* tests are done using the lifted interpolating wavelet, hereafter called LI3, that has five vanishing polynomial moments. The LI3 wavelet and its Fourier transform are shown in Fig. 1. For a more in-depth discussion on the construction of these wavelets the reader is referred to the following papers: Sweldens (1996), Sweldens (1998), Vasilyev & Bowman (2000). For a more general discussion of wavelets the following references can be consulted: Daubechies (1992), Mallat (1999).

3. Coherent Vortex Simulation

In a CVS the vorticity field is separated into two parts using a wavelet thresholding filter:

$$\vec{\omega} = \vec{\omega}_{>} + \vec{\omega}_{\leq} \tag{3.1}$$

where $\vec{\omega}_{>}$ is the filtered part of the flow defined on an adaptive grid and $\vec{\omega}_{\leq}$ is the Localized Residual Scales (LRS) field that is made as close to Gaussian white noise as possible. We use the term Localized Residual Scales to highlight the fact that there is no particular scale associated with the residual field, *i.e.*, the spectral content of the LRS varies in time and location, unlike in LES of a homogeneous flow.

The formulation for CVS then begins with the vorticity-transport equation:

$$\frac{\partial \vec{\omega}}{\partial t} = -(\vec{\mathbf{V}} \cdot \nabla)\vec{\omega} + (\vec{\omega} \cdot \nabla)\vec{\mathbf{V}} + \nu \nabla^2 \vec{\omega}. \tag{3.2}$$

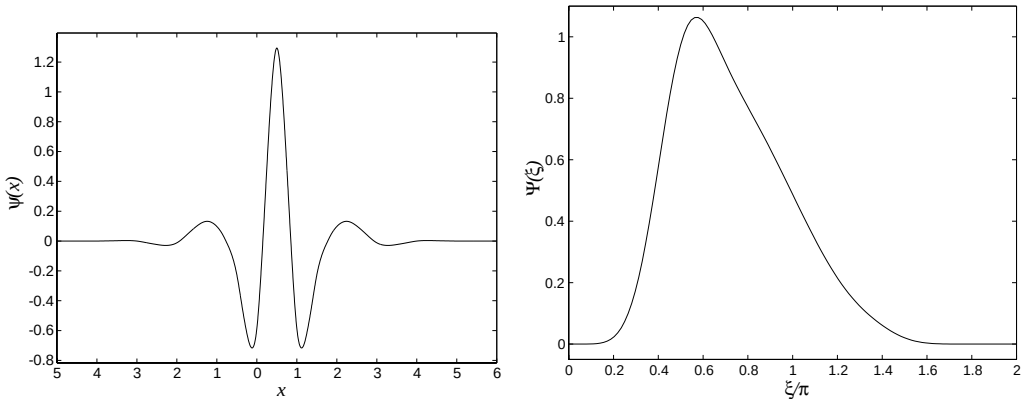

FIGURE 1. Lifted interpolating wavelet ψ and its Fourier transform $\Psi(\xi)$.

As in LES, after application of the wavelet filter we obtain the following CVS equation that describes the evolution of the filtered field:

$$\frac{\partial \vec{\omega}_>}{\partial t} = -(\vec{\mathbf{V}}_> \cdot \nabla)\vec{\omega}_> + (\vec{\omega}_> \cdot \nabla)\vec{\mathbf{V}}_> + \nu\nabla^2\vec{\omega}_> + \vec{f} \tag{3.3}$$

where

$$\vec{f} = [(\vec{\mathbf{V}} \cdot \nabla)\vec{\omega}]_> - [(\vec{\omega} \cdot \nabla)\vec{\mathbf{V}}]_> - (\vec{\mathbf{V}}_> \cdot \nabla)\vec{\omega}_> + (\vec{\omega}_> \cdot \nabla)\vec{\mathbf{V}}_> \tag{3.4}$$

is the LRS forcing that needs to be modeled. The localized nature of the LRS will have to be considered in defining residual-scale models for use with CVS. It has been shown that, when a non-linear wavelet thresholding filter is applied to a moderately high Reynolds number isotropic turbulence field, the residual field is closer to being statistically Gaussian than when a Fourier cutoff filter with the same number of modes is used. This has been shown in Farge *et al.* (1999) in 2D and will be shown in Section 4 below in 3D. Thus it is expected that the LRS can be modeled more accurately than for Fourier filtering, but this has not been proven and is a current topic of research.

Solution of the filtered vorticity equation on an adaptive grid can be done using any appropriate solution method. In Farge *et al.* (1999) a 2D CVS method was implemented using an adaptive wavelet-vaguelette algorithm (Fröhlich & Schneider (1997)). In our work we implemented a 3D CVS method using an adaptive wavelet collocation method discussed in Vasilyev & Bowman (2000), Kevlahan *et al.* (2000) that has been shown to work well in 2D flows and can be extended to 3D with little modification. This solver uses the second generation bi-orthogonal LI wavelets discussed in Section 2 and is capable of solving problems in complex domains.

The adaptive wavelet collocation method is ideally suited for the CVS of turbulent flows since every wavelet is uniquely associated with a collocation point. Thus the grid adaptation can be based on the same criterion as in coherent vortex extraction, *i.e.*, at any given time the computational grid consists of points corresponding to wavelets whose coefficients are above an optimal CVS threshold, *i.e.* we do not retain those collocation points whose wavelet coefficients were set to zero in the wavelet filtering operation. With this adaptation strategy a solution is obtained on a grid that "tracks" the coherent vortices.

The CVS method requires at least two major operations per time step:

1. Apply the wavelet thresholding filter to define the adaptive grid.

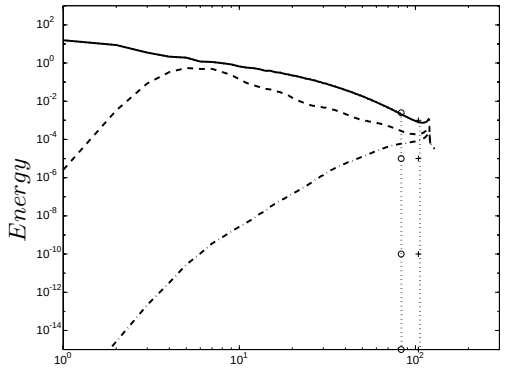

a) Spectra of forced isotropic turbulence, data set F_{256}, $Re_\lambda = 168$.

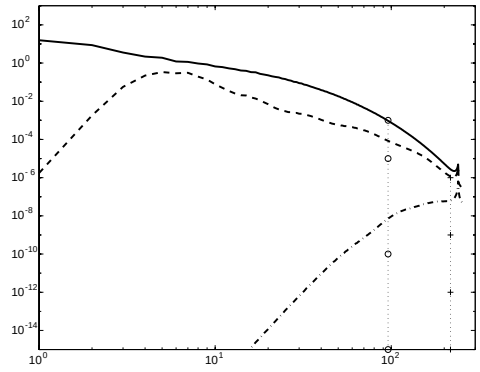

b) Spectra of forced isotropic turbulence, data set F_{512}, $Re_\lambda = 168$.

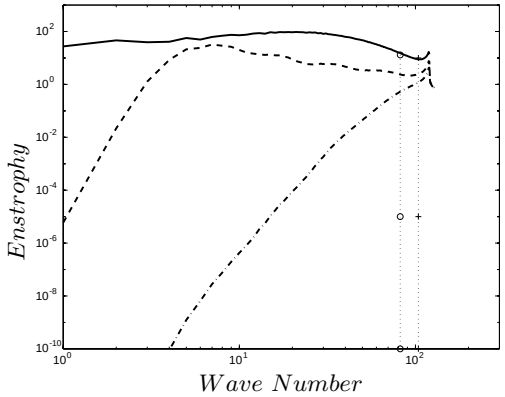

c) Enstrophy of forced isotropic turbulence, data set F_{256}, $Re_\lambda = 168$.

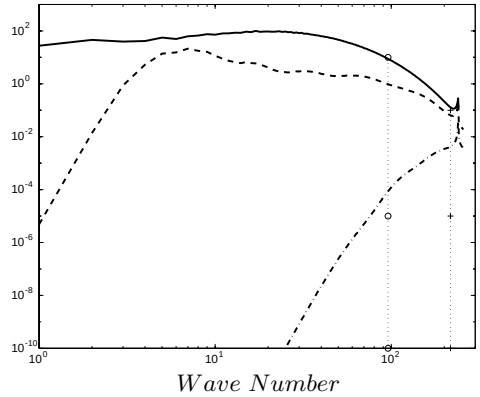

d) Enstrophy of forced isotropic turbulence, data set F_{512}, $Re_\lambda = 168$.

FIGURE 2. Energy and enstrophy spectra of forced isotropic turbulence for data sets F_{256} and F_{512}. Spectra of the full field: (———). Spectra of the LRS field after optimal wavelet compression using DB6 wavelets: (—·—) and LI3 wavelets: (– – –). The Fourier cutoff filter with compression equivalent to optimal DB6 wavelet filter: (·· + ··) and to optimal LI3 wavelet filter: (·· ○ ··).

2. Numerically solve Eq. 3.3 on the adaptive grid.

Using the same wavelets for these two steps would be most computionally efficient. This is why we are interested in investigating the use of second generation bi-orthogonal wavelets for coherent vortex extraction.

Although in this paper we do not discuss the solution of the wavelet filtered vorticity equation (3.3), it is good to point out that since the CVS equations are solved on an adaptive grid, we cannot use spectral methods for the solution of the Poisson equation that relates the vorticity field to the velocity field. The development of an efficient wavelet collocation based method for the solution of the Poisson equation on an adaptive grid is currently a subject of study.

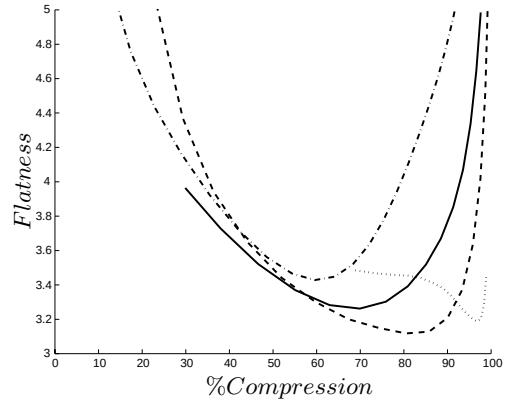

a) Flatness ($< \omega^4 > / < \omega^2 >^2$). (Note: Flatness of a Gaussian field is 3.0.)

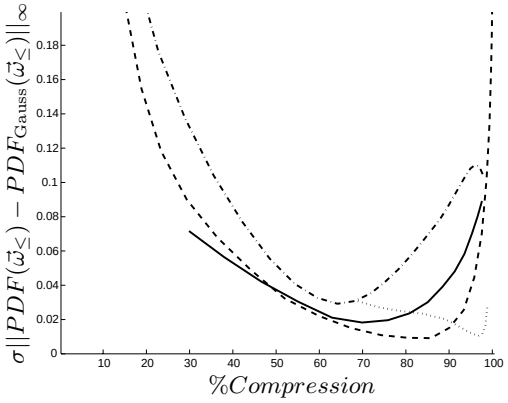

b) L_∞ Error between LRS and Gaussian PDFs with the same mean and variance.

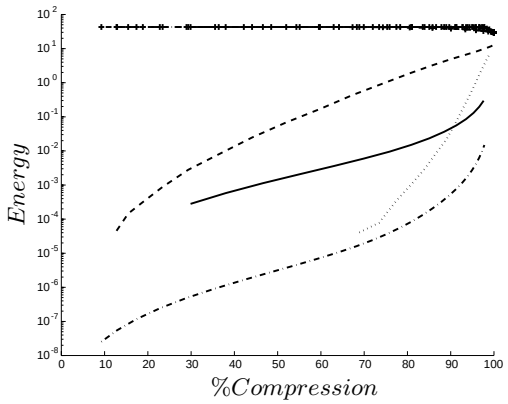

c) Total kinetic energy.

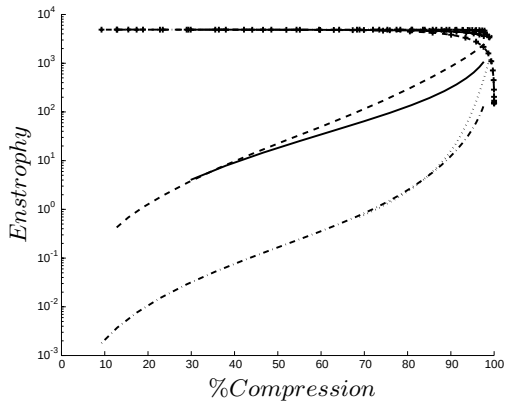

d) Total enstrophy.

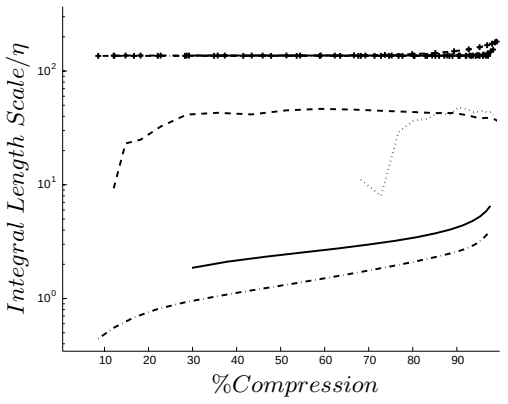

e) Velocity integral length scale.

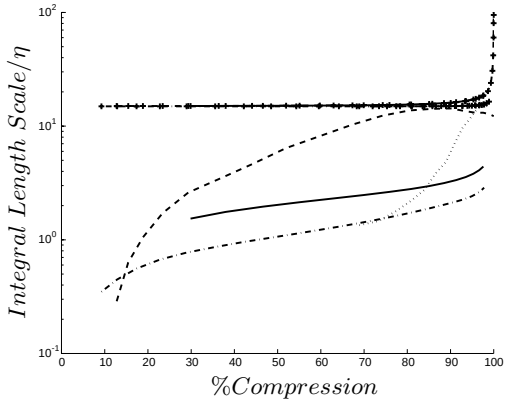

f) Vorticity integral length scale.

FIGURE 3. Filtered and LRS field statistics for isotropic turbulence fields F_{256} and F_{512} after application of wavelet thresholding filter using LI3 and DB6 wavelets. LRS field statistics of F_{256} using DB6 wavelets: (———) and LI3 wavelets: (– – – –). LRS field statistics of F_{512} using DB6 wavelets: (—·—) and LI3 wavelets: (·····). In plots c) through f) the lines with (+) are the same statistics for the filtered fields. (Note: The filtered statistics are mostly constant until almost 100% compression so these lines are obscured by each other.)

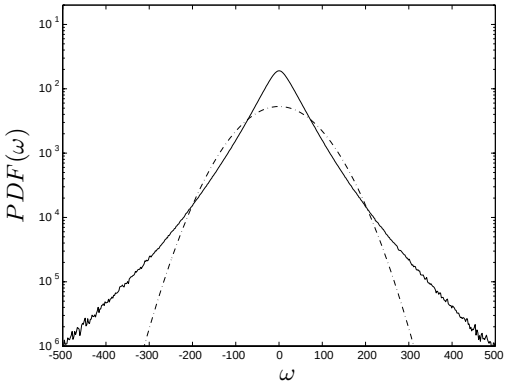

FIGURE 4. PDF of forced isotropic turbulence field F_{256}: (———). Gaussian PDF with same mean and variance: (—·—).

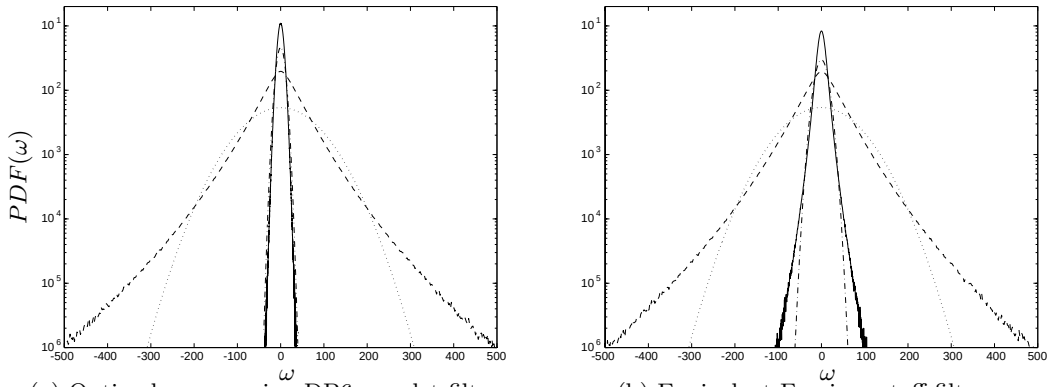

(a) Optimal compression DB6 wavelet filter. (b) Equivalent Fourier cutoff filter.

FIGURE 5. PDF of forced isotropic turbulence field F_{256} using DB6 wavelet filter at 50% compression (a) and Fourier cutoff filter at the equivalent compression (b). Filtered field: (– – – –), with its associated Gaussian: (·····). LRS field: (———), with its associated Gaussian: (—·—).

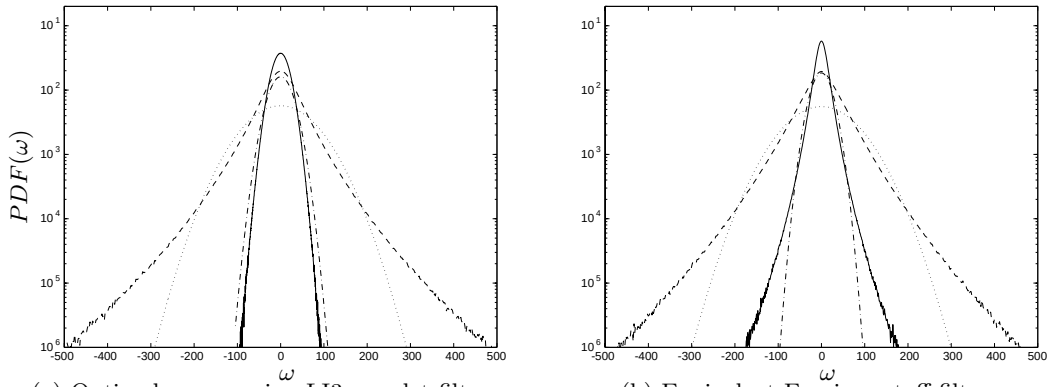

(a) Optimal compression LI3 wavelet filter. (b) Equivalent Fourier cutoff filter.

FIGURE 6. PDF of forced isotropic turbulence field F_{256} using LI3 wavelet filter at 86% compression (a) and Fourier cutoff filter at the equivalent compression (b). Filtered field: (– – – –), with its associated Gaussian: (·····). LRS field: (———), with its associated Gaussian: (—·—).

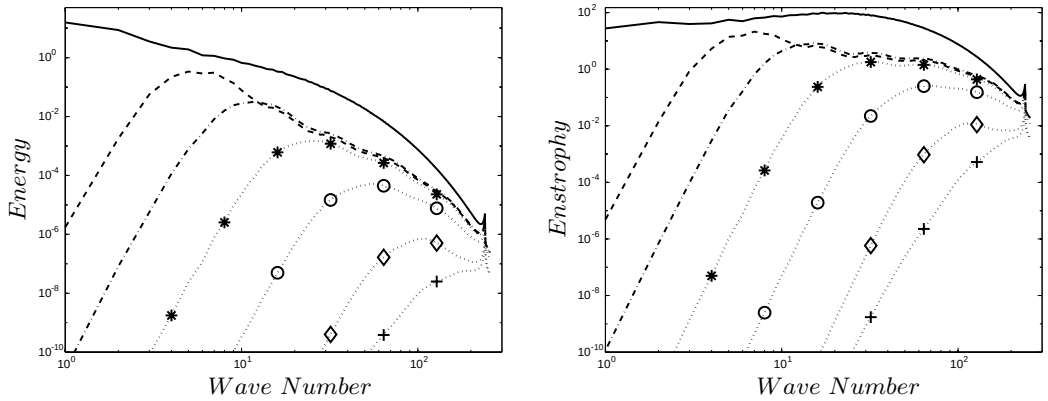

FIGURE 7. Energy and enstrophy spectra of forced isotropic turbulence data set F_{512}, $Re_\lambda = 168$. Spectra of the full field: (———). LRS field spectra after optimal decomposition with DB6 wavelets with 6 levels: (·· + ··). The rest of the lines are the LRS field spectra after optimal wavelet compression with LI3 wavelets with varying number of decomposition levels: 2 levels: (·· ◇ ··), 3 levels: (·· ○ ··), 4 levels: (·· ∗ ··), 5 levels: (—·—), 6 levels: (– – – –).

4. Results and discussion

For the CVS method to work, we want to find the optimal value of ϵ such that the wavelet filter decomposes the vorticity field into a filtered field that contains all the coherent vortices of significant energy and an LRS field that is as close to Gaussian white noise as possible. One way to find the optimal value of ϵ is to use Donoho's de-noising theorem (Donoho (1993)) that states that if there is a Gaussian white-noise component in the vorticity field and somehow we know its variance, we can extract it using wavelet thresholding with orthogonal wavelets. Donoho's de-noising theorem says that the threshold required to extract the Gaussian white-noise component is $\epsilon_{\text{Donoho}} = \sqrt{2\sigma^2 \log(N)}$, where σ^2 is the variance of the Gaussian white noise and N is the number of points in the field. However, the variance of the Gaussian white-noise component of the vorticity field is not known. One way to find the LRS field with maximum Gaussianity is to iterate on $\epsilon_{n+1} = \sqrt{2\sigma^2_{\text{LRS}_n} \log(N)}$, with σ_{LRS_0} taken as the variance of the full field (Farge *et al.* (1999)). If there exists an LRS field that is Gaussian white noise, then the iterative process should converge to ϵ_{Donoho}. However, since Donoho's theorem does not directly apply to bi-orthogonal wavelets, another way to find the optimal ϵ needs to be found.

In order to prove the existence of an optimal value for ϵ for second generation wavelets and, possibly, find an efficient way of finding it, a series of parametric studies were performed by varying ϵ to achieve a range of compression from 0% to 100%. The results for the second generation bi-orthogonal (LI) wavelets were compared to the orthogonal Daubechies DB6 wavelets (Daubechies (1992)). Both of these wavelets have five vanishing moments and an effective filter length of 12. We carried out these parametric studies using a number of forced and decaying isotropic turbulence fields from a database of spectral DNS. Due to space restrictions the results from only two representative forced isotropic turbulence fields F_{256} and F_{512} ($Re_\lambda = 168$) will be presented in detail. We also will refer to two decaying isotropic turbulence fields CBC_{256} and CBC_{512} ($Re_\lambda = 55$). More detailed information about these data sets can be found in Jimenez & Wray (1993).

The energy and enstrophy spectra of data sets F_{256} and F_{512} are shown in Fig. 2. Figure 3 shows various statistical quantities (as a function of compression) of the filtered and LRS fields after wavelet thresholding with DB6 and LI3 wavelets. In this paper we define

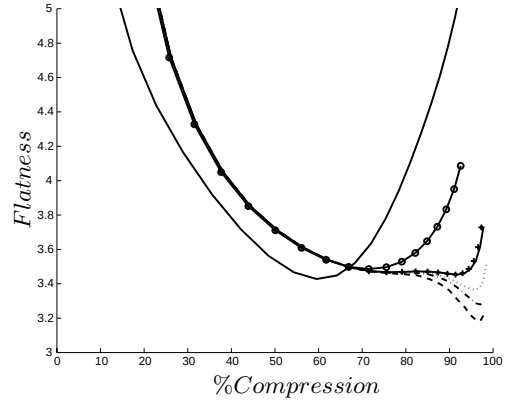

a) Flatness ($< \omega^4 > / < \omega^2 >^2$). (Note: Flatness of a Gaussian field is 3.0.)

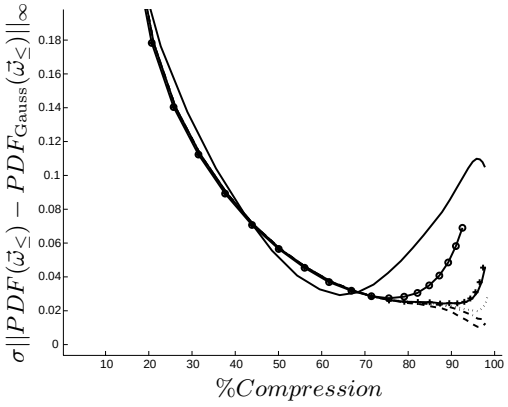

b) L_∞ error between LRS field and a Gaussian PDFs with the same mean and variance.

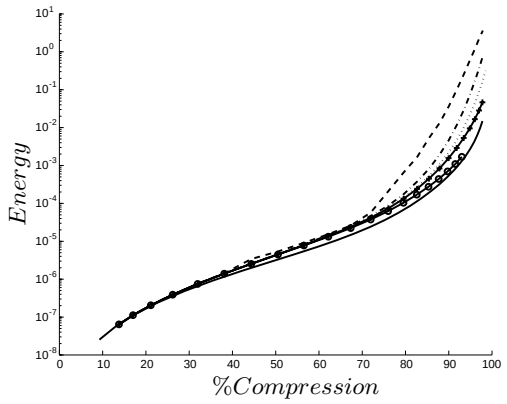

c) Total kinetic energy.

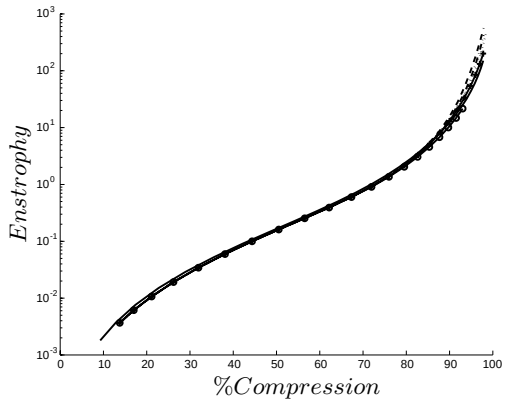

d) Total enstrophy.

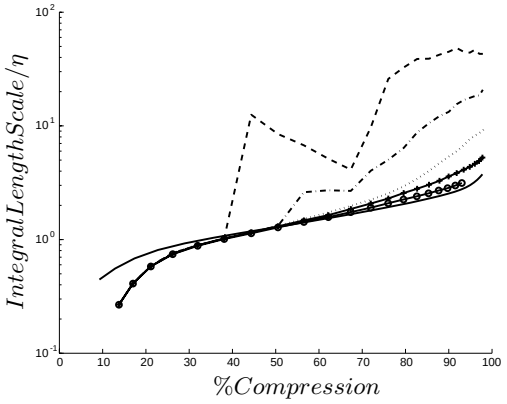

e) Velocity Integral Length Scale.

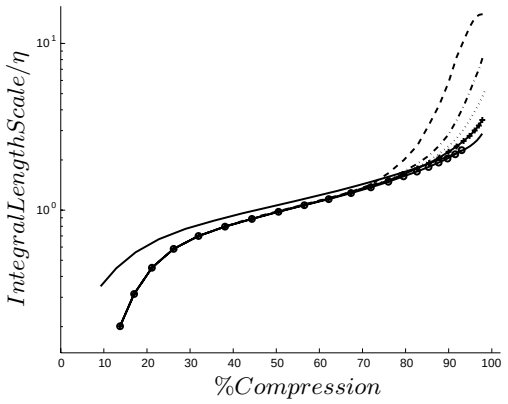

f) Vorticity integral length scale.

FIGURE 8. Comparison of LRS field statistics after wavelet filtering of forced isotropic turbulence data set F_{512}, $Re_\lambda = 168$. LRS field statistics using DB6 wavelets with 6 levels: (———) The rest of the lines are the LRS field statistics after optimal wavelet compression with LI3 wavelets with varying number of decomposition levels: 2 levels: (—●—), 3 levels: (·· + ··), 4 levels: (·····), 5 levels: (—·—), 6 levels: (– – – –).

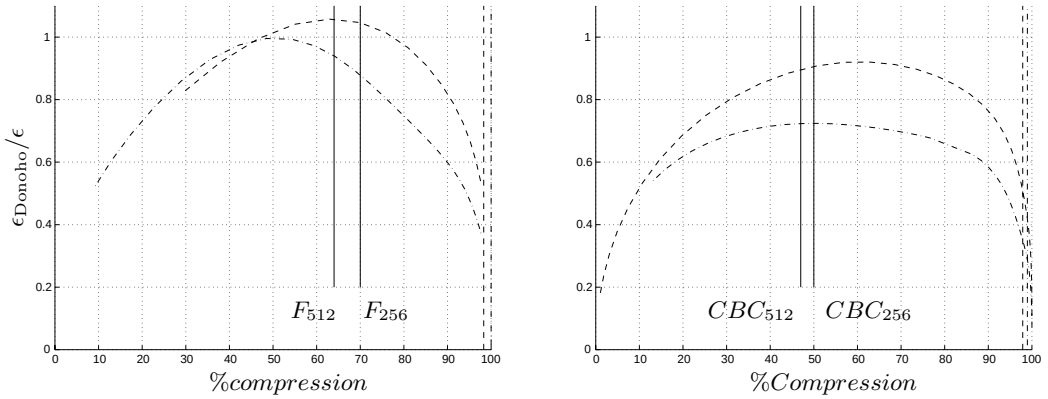

a) Forced isotropic turbulence fields F_{256}: (– – – –) and F_{512}: (— · —).

b) Decaying isotropic turbulence fields CBC_{256}: (– – – –) and CBC_{512}: (— · —)

FIGURE 9. Wavelet threshold from Donoho's de-noising theorem scaled by the actual threshold used with DB6 wavelet thresholding. The % compression at minimum flatness is marked for each field by solid vertical lines. The resulting compression when Donoho's theorem is applied to the full vorticity field is shown by vertical lines, 256^3 field: (– – – –), 512^3 field: (— · —).

the compression as $\frac{N_>}{N} \times 100\%$, where $N_>$ is the number of retained wavelet coefficients for a given threshold ϵ. In Fig. 3a we can see that in each case there is a minimum for the flatness. This minimum is interpreted as the optimal wavelet compression of the field in terms of Gaussianity of the LRS field. Figure 3b shows the scaled L_∞ error between the PDF of the LRS field and a Gaussian PDF with the same mean and variance. It can be seen that the minima in Figs. 3a and 3b coincide, showing that the flatness is a good indicator of the Gaussianity of the field. It can also be seen from these plots that the optimal compression of both fields is better for the LI3 wavelets than the DB6 wavelets. However, this does not show the whole story. In Fig. 3c we see that the total kinetic energy in the LRS field is greater for both fields when the LI3 wavelets are used, while the difference is much less if we look at the total enstrophy in Fig. 3d. It is significant that the velocity (Fig. 3e) and vorticity (Fig. 3f) integral length scales of the LRS field are considerably larger for the LI3 wavelets. This indicates that the LI3 wavelets are extracting a more Gaussian LRS field at a higher optimal compression ratio, but this LRS field is more coherent than that from DB6 wavelets. Since the goal of the CVS approach is to extract an incoherent Gaussian white noise, this is considered unfavorable for the LI3 wavelets.

It is also interesting to note that for the LI3 wavelets the optimal compression is considerably greater for the F_{512} data set when compared to the F_{256} case (see Figs. 2a and 2b). In fact, the number of wavelets used to represent the filtered fields is approximately the same for both F_{256} and F_{512} data sets, which means that additional scales are approximated with virtually no extra cost. However, this is not true for the DB6 wavelet filter.

Figure 4 shows the PDF of vorticity for data set F_{256} and the Gaussian PDF with the same mean and variance. In Fig. 5, for data set F_{256}, the PDFs of the filtered and LRS vorticity fields at optimum wavelet compression using DB6 wavelets are compared to those from a Fourier cutoff filter that retains the same number of modes. The difference in the Gaussianity of the LRS field of the two filters can most clearly be seen in the tails.

With both LI3 and DB6 wavelet thresholding the LRS field is clearly more Gaussian in the tails than the residuals from the Fourier cutoff filter. In both cases there is a large difference around zero between the PDF of the LRS field and the corresponding Gaussian PDF; this difference dominates the L_∞ error.

As a possible way to improve the performance of the LI3 wavelets for coherent vortex extraction, we studied the effect of diminishing the number of multiresolution levels used in the wavelet transform. For a resolution of 512^3, the maximum number of levels that can be used with the LI3 and DB6 wavelets before the support of the scaling functions start to overlap at the coarsest level is 6 (see Daubechies (1992) for a more in-depth discussion of the wavelet transform). Figure 7 shows the energy and enstrophy spectra for data set F_{512} and the LRS fields after optimal wavelet compression using DB6 wavelets with 6 levels in the transform, as in Fig. 3. Also shown are the energy and enstrophy spectra of the LRS fields after optimal wavelet compression using LI3 wavelets with 2 through 6 levels of resolution. Note that, as the number of levels of resolution used in the LI3 wavelet transform decreases, the LRS field contains less energy and approaches the energy retained by the DB6 wavelet filter. In Fig. 8 we compare the the same statistics as we did in Fig. 3 for the DB6 wavelet transform to the LI3 wavelet transform with a range of levels of resolution. It can be easily seen in Figs. 8a and 8b that as the number of levels used in the wavelet transform decreases, the LRS field becomes less Gaussian. We also see that the LI3 wavelet transform with four levels results in a LRS field with better Gaussianity (compared to the DB6 wavelet filter) with an optimal compression ratio of 96% vs. 60% for the DB6 wavelet filter. Comparing the total energy and enstrophy (Figs. 8c and 8d) for the LI3 wavelet transform with four levels of resolution to the DB6 wavelet transform, it can be clearly seen that the difference in total kinetic energy is minimal and total enstrophy is almost identical. An interesting trend can be seen in the velocity (Fig. 8e) and vorticity (Fig. 8f) integral length scales: using fewer levels in the LI3 wavelet transform results in less coherence of the LRS field.

Finally, let us discuss the application of Donoho's de-noising theorem to find the optimal wavelet compression using DB6 orthogonal wavelets. Figure 9 shows the normalized threshold coefficient ($\epsilon_{\text{Donoho}}/\epsilon$) derived from Donoho's de-noising theorem for the LRS field vs. the % compression of the field. Recall, that a given vorticity field ϵ_{Donoho}, which is a function of the variance of the LRS field, is uniquely defined by the value ϵ used in wavelet filter. The solid vertical lines show the optimal compression as determined by the minimum flatness and L_∞ error. We can see that because the LRS fields are never really Gaussian white noise, the optimal compression and the points where $\epsilon_{\text{Donoho}}/\epsilon = 1.0$ do not coincide. In fact, for the decaying isotropic turbulence data sets CBC_{256} and CBC_{512}, which have a lower Re_λ ($Re_\lambda = 55$), $\epsilon_{\text{Donoho}}/\epsilon$ never reaches 1.0. We have also superimposed vertical lines that show the optimal compression ratio obtained if Donoho's de-noising theorem is applied using the variance of the full field. We can see that this results in a much higher compression than at the point of maximum Gaussianity (see Fig. 3).

5. Conclusions

The performance of the bi-orthogonal second generation wavelet transform and the orthogonal wavelet transform using Daubechies wavelets with the same number of vanishing moments is compared in *a priori* tests using a spectral DNS database of isotropic turbulence fields: 256^3 and 512^3 DNS of forced homogeneous turbulence ($Re_\lambda = 168$) and 256^3 and 512^3 DNS of decaying homogeneous turbulence ($Re_\lambda = 55$). The results of

these *a priori* tests indicate that lifted interpolating bi-orthogonal wavelets are able to extract a more Gaussian LRS field at a higher optimal compression ratio than orthogonal DB wavelets. However the extracted LRS field is more coherent than when using orthogonal DB wavelets. This problem can be overcome by reducing the number of levels of resolution in the wavelet transform. In addition, it was found that the optimal wavelet compression did not coincide with the theoretical compression predicted by Donoho's de-noising theorem. The most probable explanation for this is that the LRS field never actually becomes Gaussian white noise.

Future work in this area will include comparing the second generation wavelets wavelets to other orthogonal wavelets and implementing the CVS approach in the adaptive second generation wavelet collocation method.

Acknowledgments

We would like to thank the Center for Turbulence Research and NASA Ames for their support that made this work possible.

REFERENCES

Cohen, A., Daubechies, I., & Feauveau, J. 1992 Bi-orthogonal bases of compactly supported wavelets. *Comm. Pures and Appl. Math.* **45**, 485-560.

Daubechies, I. 1988 Orthonormal bases of compactly supported wavelets. *Comm. Pure and Appl. Math.* **41**, 909-996.

Daubechies, I. 1992 *Ten Lectures on Wavelets*. no. 61 in CBMS-NSF Series in Applied Mathematics, SIAM, Philadelphia.

Donoho, D. 1993 Unconditional bases are optimal bases for data compression and for statistical estimation. *Appl. Comput. Harmon. Anal.* **1**, 100-115.

Farge, M., Schneider, K., & Kevlahan, N. 1999 Non-Gaussianity and coherent vortex simulation for two-dimensional turbulence using an adaptive orthogonal wavelet basis. *Phys. Fluids.* **11**(8), 2187-2201.

Fröhlich, J. & Schneider, K. 1997 An adaptive wavelet-vaguelette algorithm for the solution of pdes. *J. Comput. Phys.*. **130**, 174-190.

Jiménez, J. & Wray, A. A. 1993 The structure of intense vorticity in isotropic turbulence. *J. Fluid Mech.* **255**, 65-90.

Kevlahan, N. K. R., Vasilyev, O. V., & Cherhabili, A. 2000 An adaptive wavelet method for turbulence in complex geometries. In *Proceedings of the 16th IMACS World Congress 2000*, 411-39.pdf, IMACS.

Mallat, S. G. 1999 *A Wavelet Tour of Signal Processing*. Academic Press, Paris.

Sweldens, W. 1996 The lifting scheme: A custom-design construction of biorthogonal wavelets. *Appl. Comput. Harmon. Anal.* **3**(2), 186-200.

Sweldens, W. 1998 The lifting scheme: A construction of second generation wavelets. *SIAM J. Math. Anal.* **29**(2), 511-546.

Vasilyev, O. V. & Bowman, C. 2000 Second generation wavelet collocation method for the solution of partial differential equations. To appear in *J. Comp. Phys.*